

Supplementary Information

Convenient Access to Functionalized Non-Symmetrical Atropisomeric 4,4'-Bipyridines

Emmanuel Aubert ¹, Emmanuel Wenger ¹, Paola Peluso ^{2,*} and Victor Mamane ^{3,*}

¹ Université de Lorraine, CNRS, CRM2, F-54000 Nancy, France; emmanuel.aubert@univ-lorraine.fr (E.A.); emmanuel.wenger@univ-lorraine.fr (E.W.)

² Institute of Biomolecular Chemistry ICB, CNR, Secondary branch of Sassari, Traversa La Crucca 3, Regione Baldinca, Li Punti, 07100 Sassari, Italy

³ Strasbourg Institute of Chemistry, UMR CNRS 7177, Team LASYROC, 1 rue Blaise Pascal, University of Strasbourg, 67008 Strasbourg CEDEX, France

* Correspondence: paola.peluso@cnr.it (P.P.); vmamane@unistra.fr (V.M.); Tel.: +39-079-2841218 (P.P.); +33-3-68851612 (V.M.)

Table of Contents

| Section | Table Caption | Page |
|---------|--------------------------|------|
| S1 | NMR spectra | 2 |
| S2 | X-Ray Diffraction | 20 |
| S3 | Theoretical Calculations | 24 |

S1. NMR Spectra

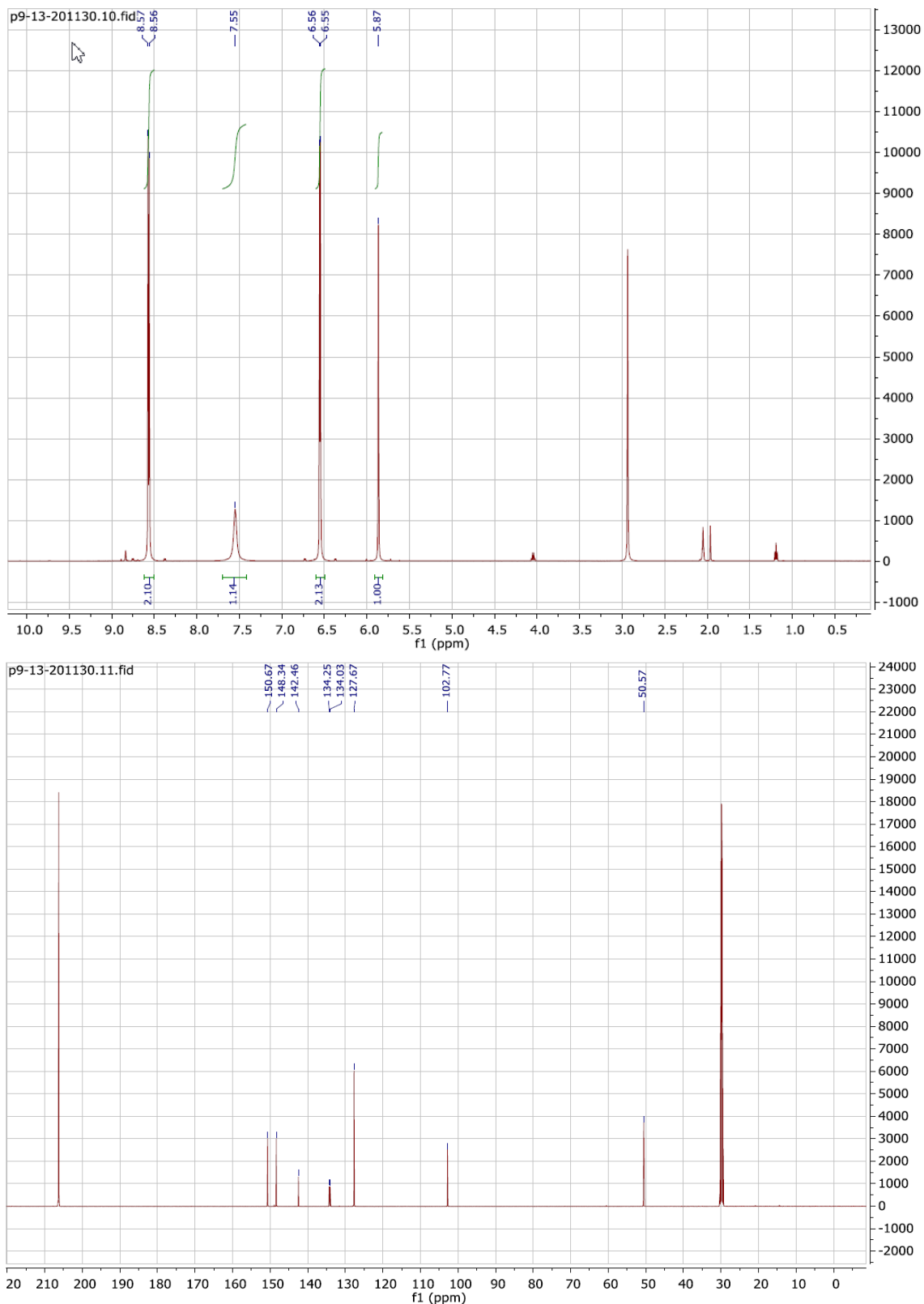


Figure S1. 3,3',5,5'-Tetrachloro-1,4-dihydro-4,4'-bipyridine (**12**).

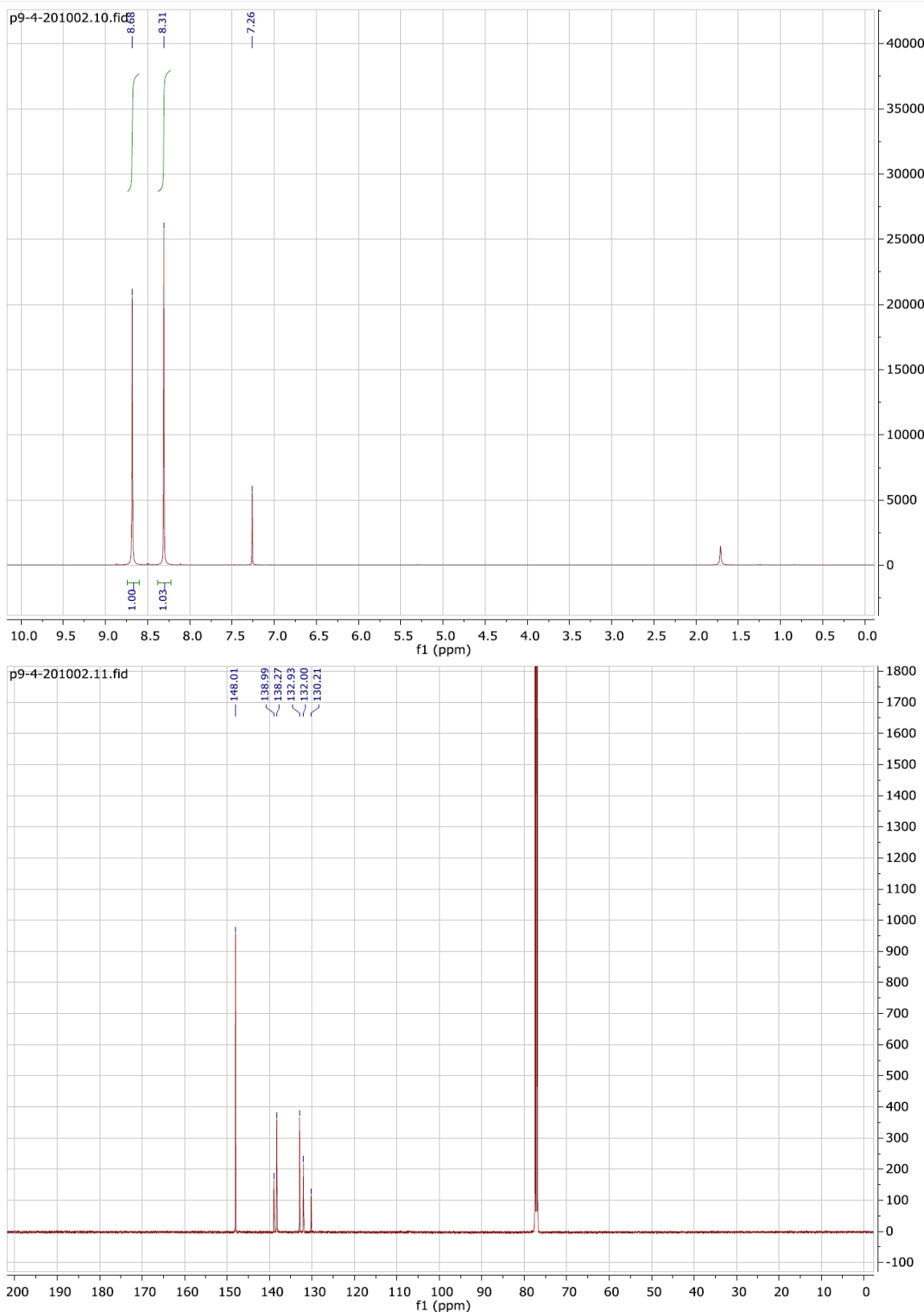


Figure S2. 3,3',5,5'-Tetrachloro-[4,4'-bipyridine] 1-oxide (**13**).

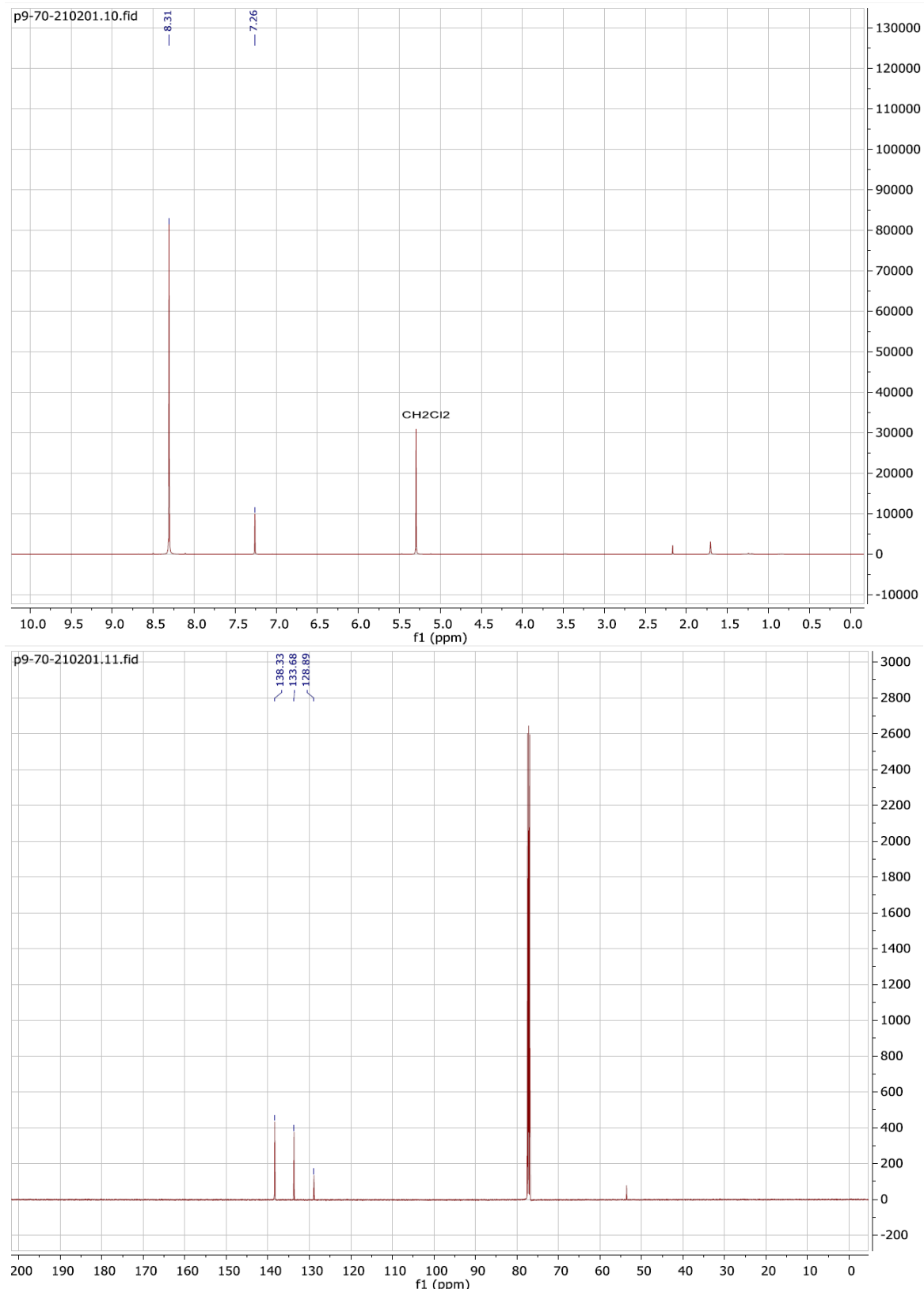


Figure S3. 3,3',5,5'-Tetrachloro-[4,4'-bipyridine] 1,1'-dioxide (**14**).

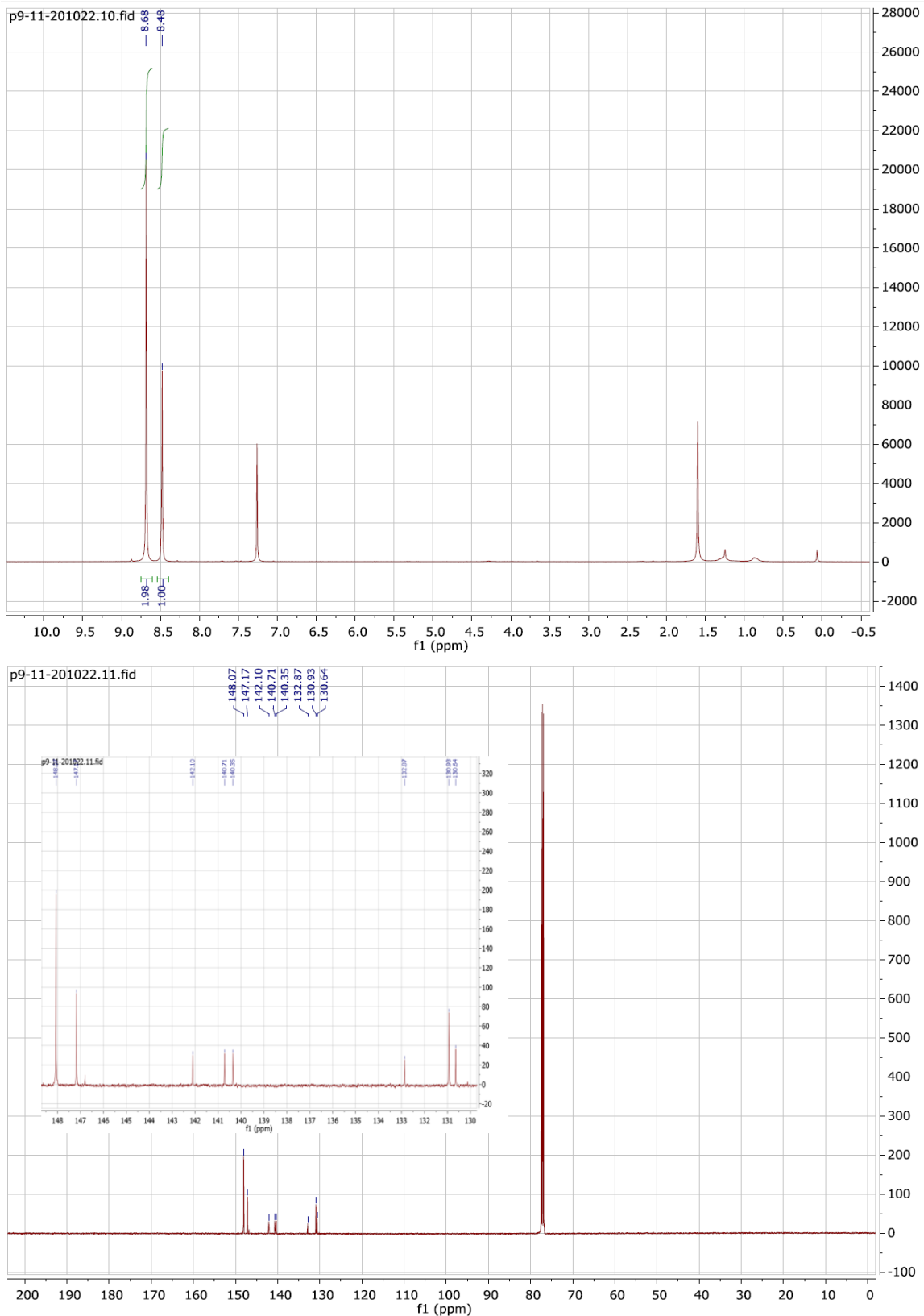


Figure S4. 2-Bromo-3,3',5,5'-tetrachloro-4,4'-bipyridine (15).

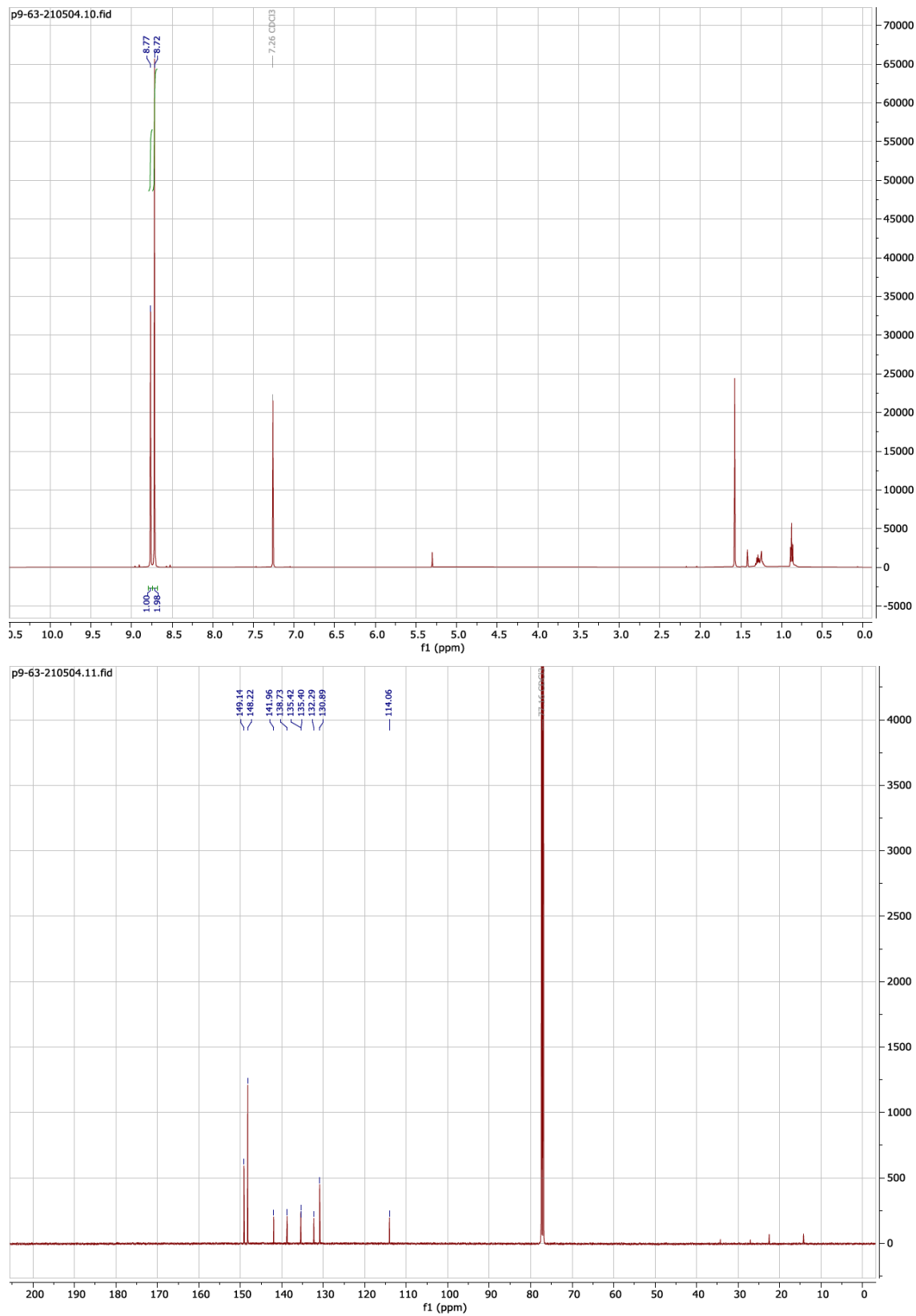


Figure S5. 3,3',5,5'-Tetrachloro-[4,4'-bipyridine]-2-carbonitrile (**16**).

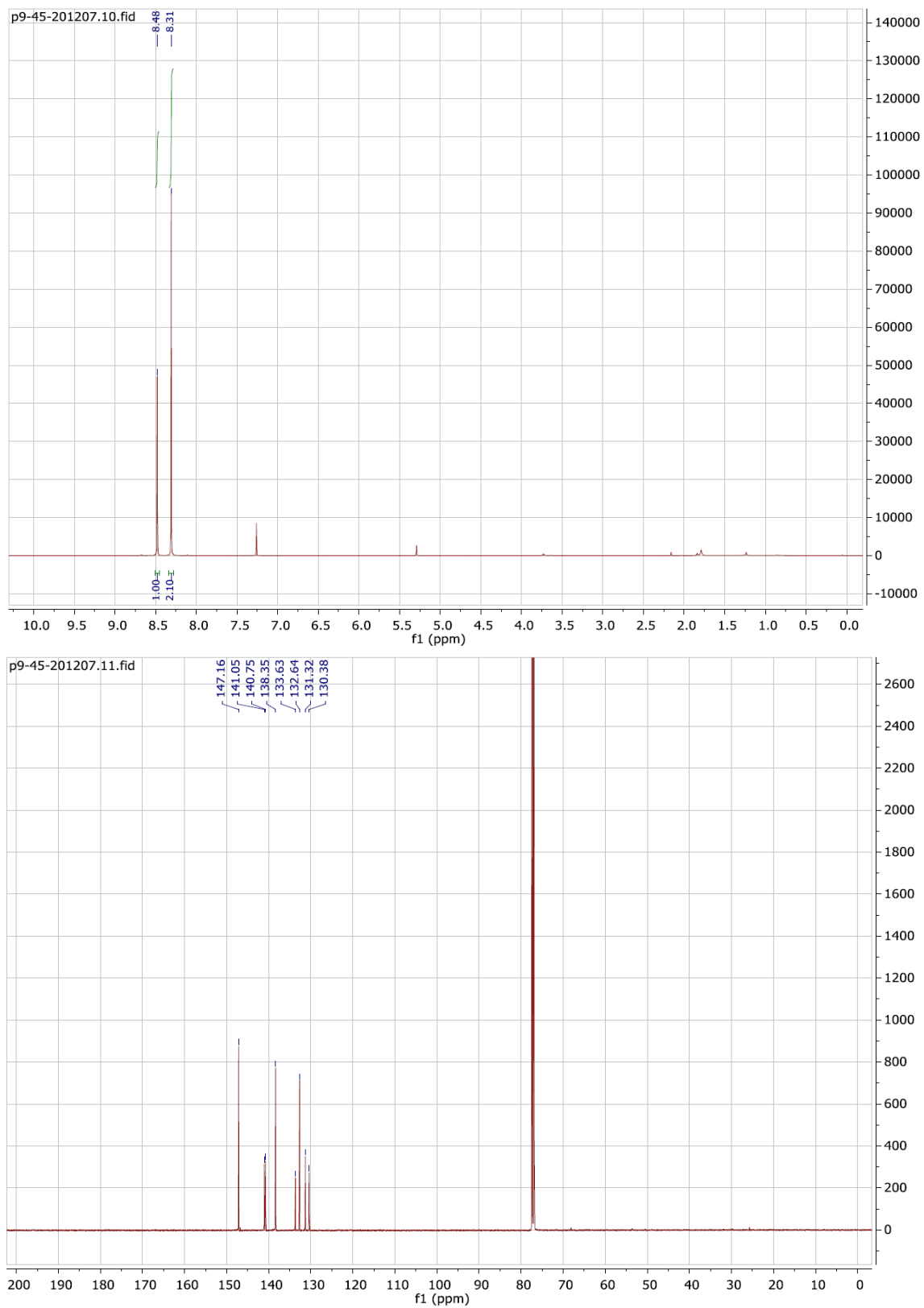


Figure S6. 2-Bromo-3,3',5,5'-tetrachloro-[4,4'-bipyridine] 1-oxide (**17**).

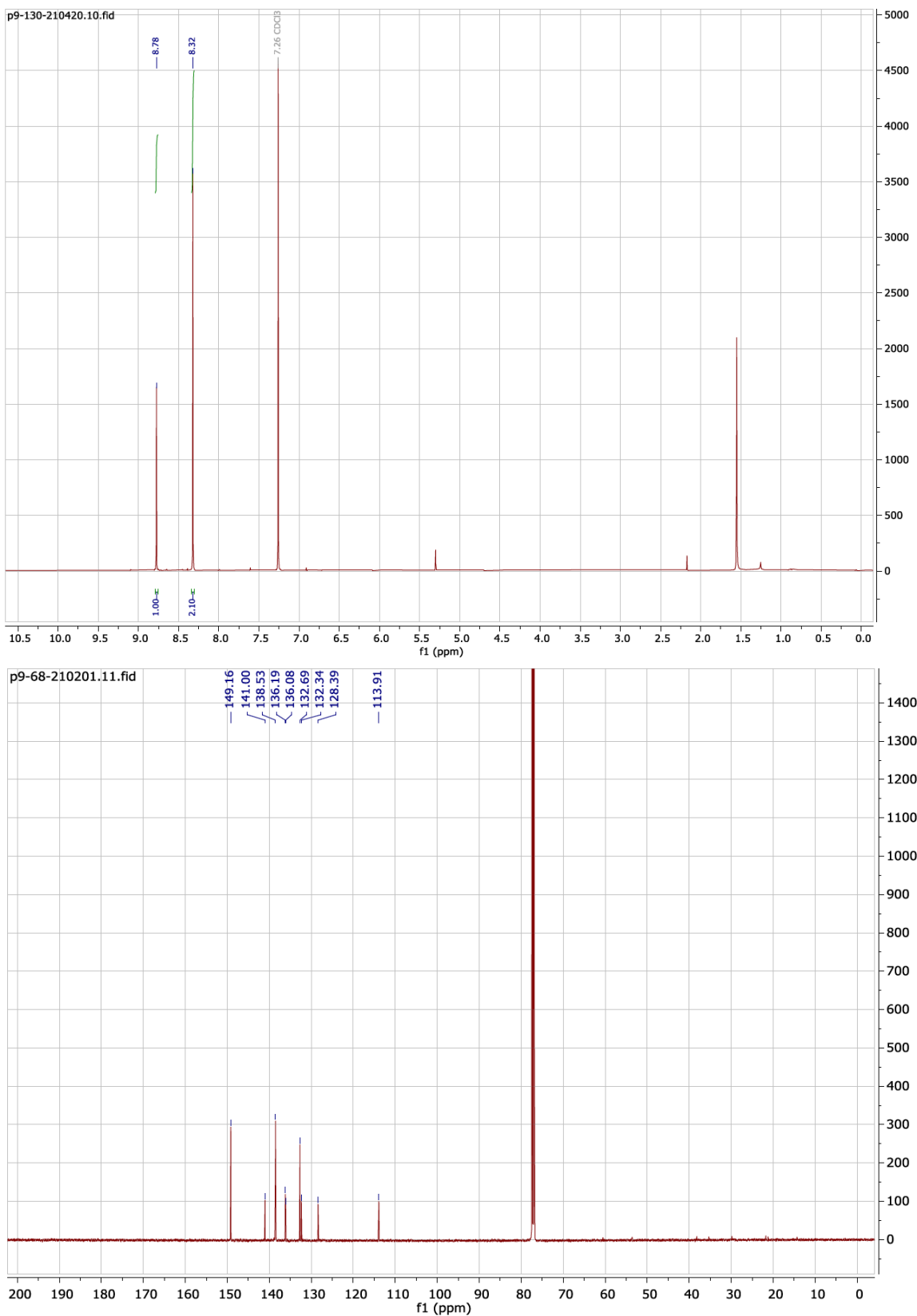


Figure S7. 3,3',5,5'-Tetrachloro-2'-cyano-[4,4'-bipyridine] 1-oxide (**18**).

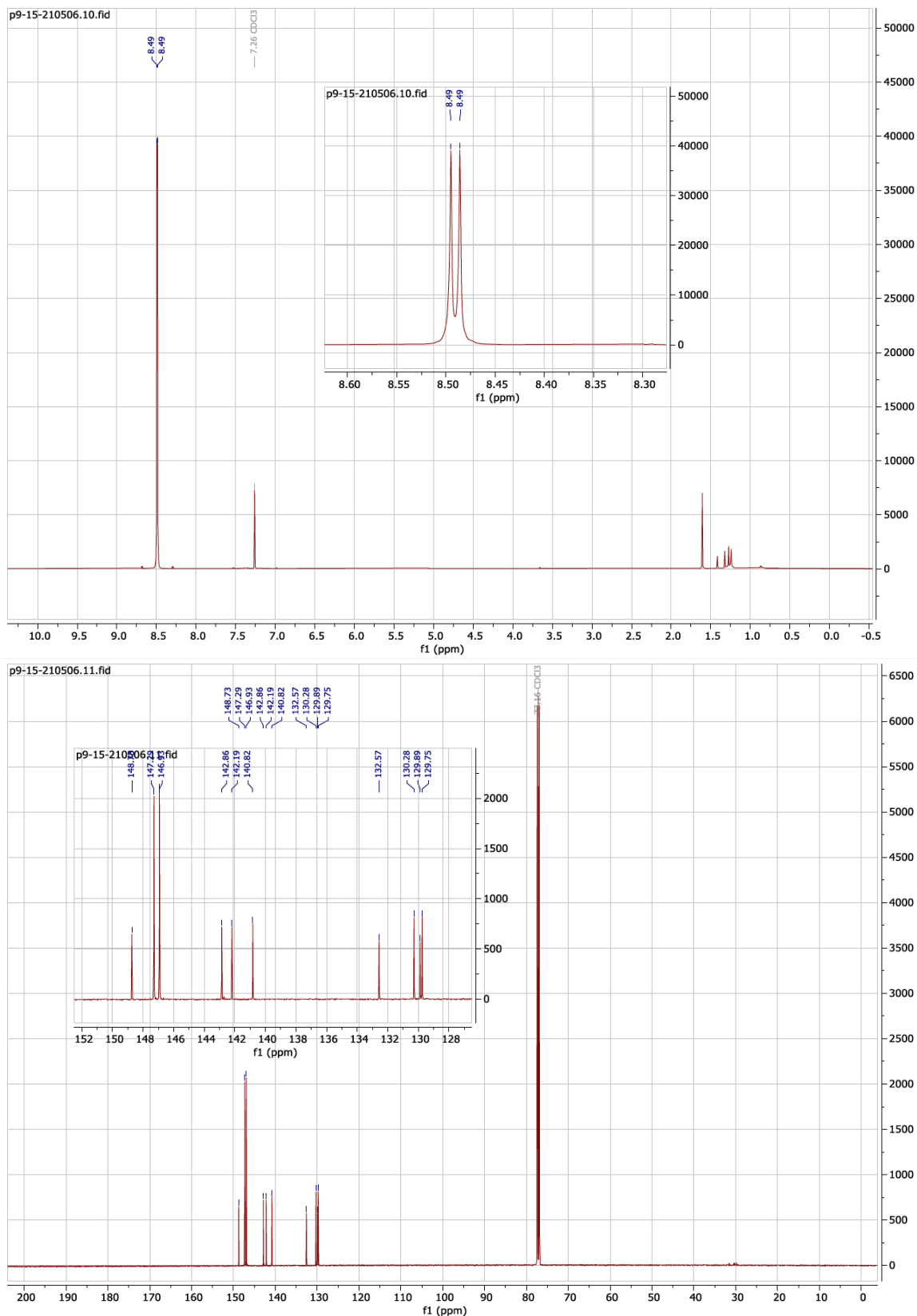


Figure S8. 2-Bromo-2',3,3',5,5'-pentachloro-4,4'-bipyridine (**19**).

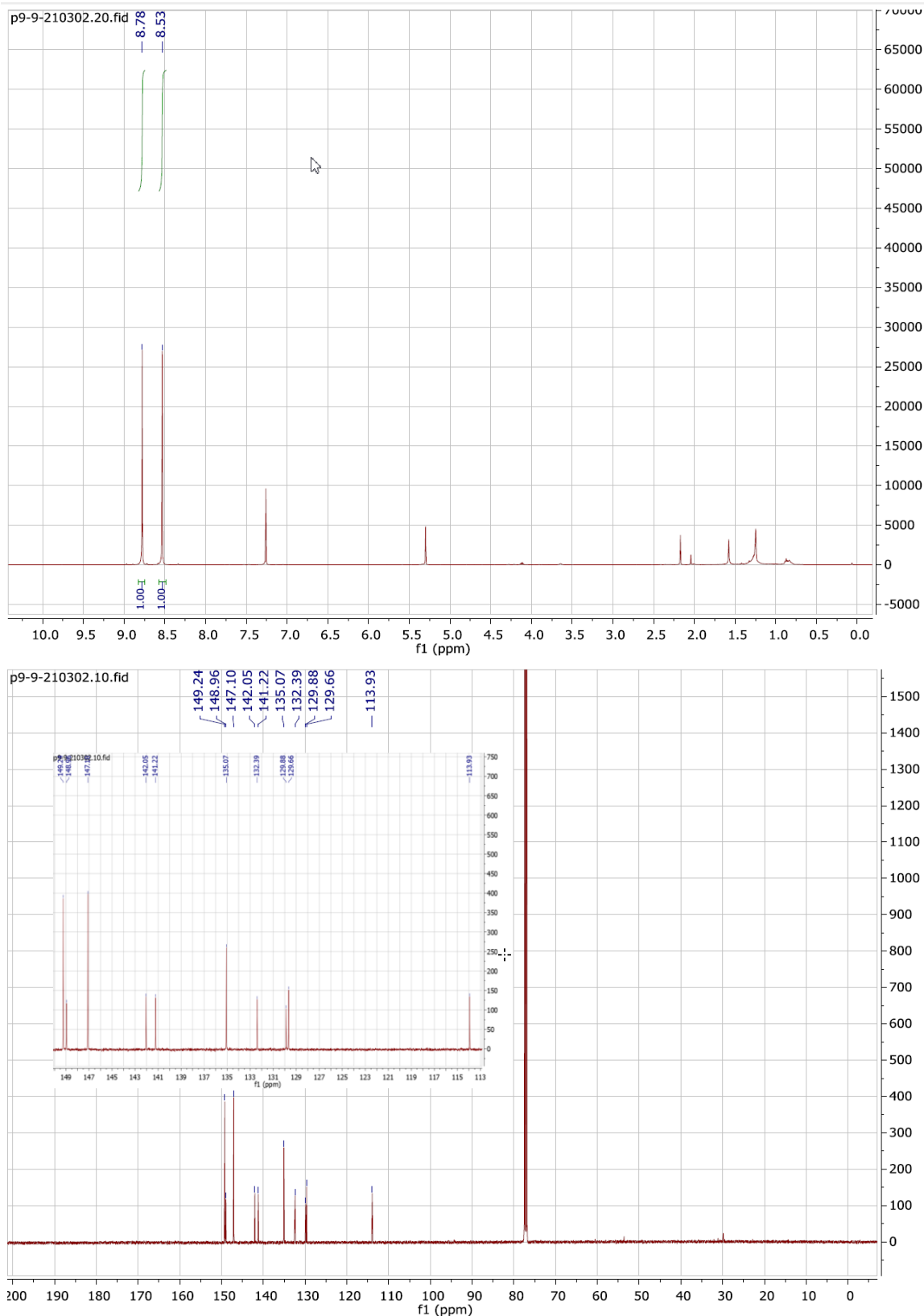


Figure S9. 2',3,3',5,5'-Pentachloro-[4,4'-bipyridine]-2-carbonitrile (**20**).

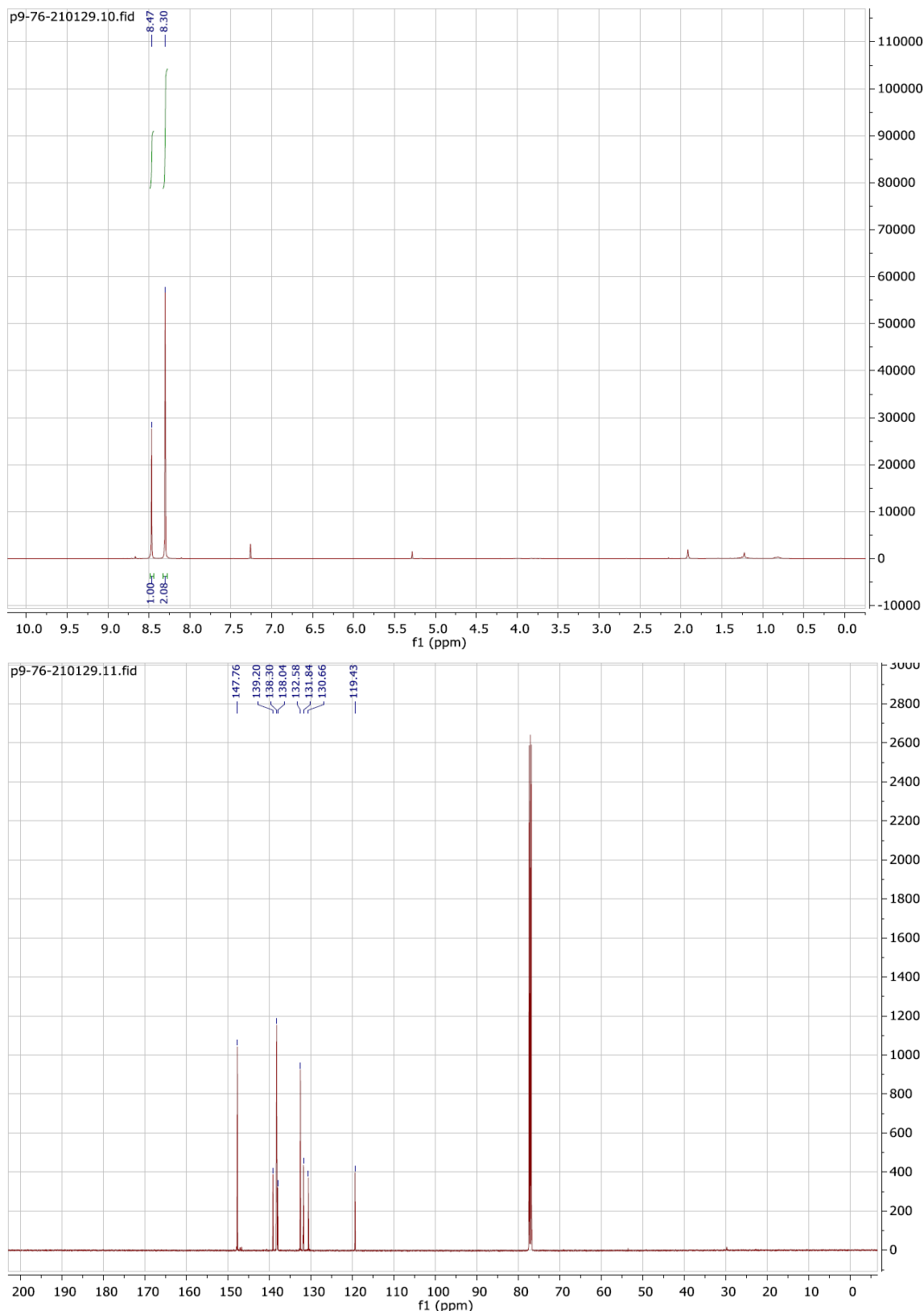


Figure S10. 3,3',5,5'-Tetrachloro-2'-iodo-[4,4'-bipyridine] 1-oxide (**21**).

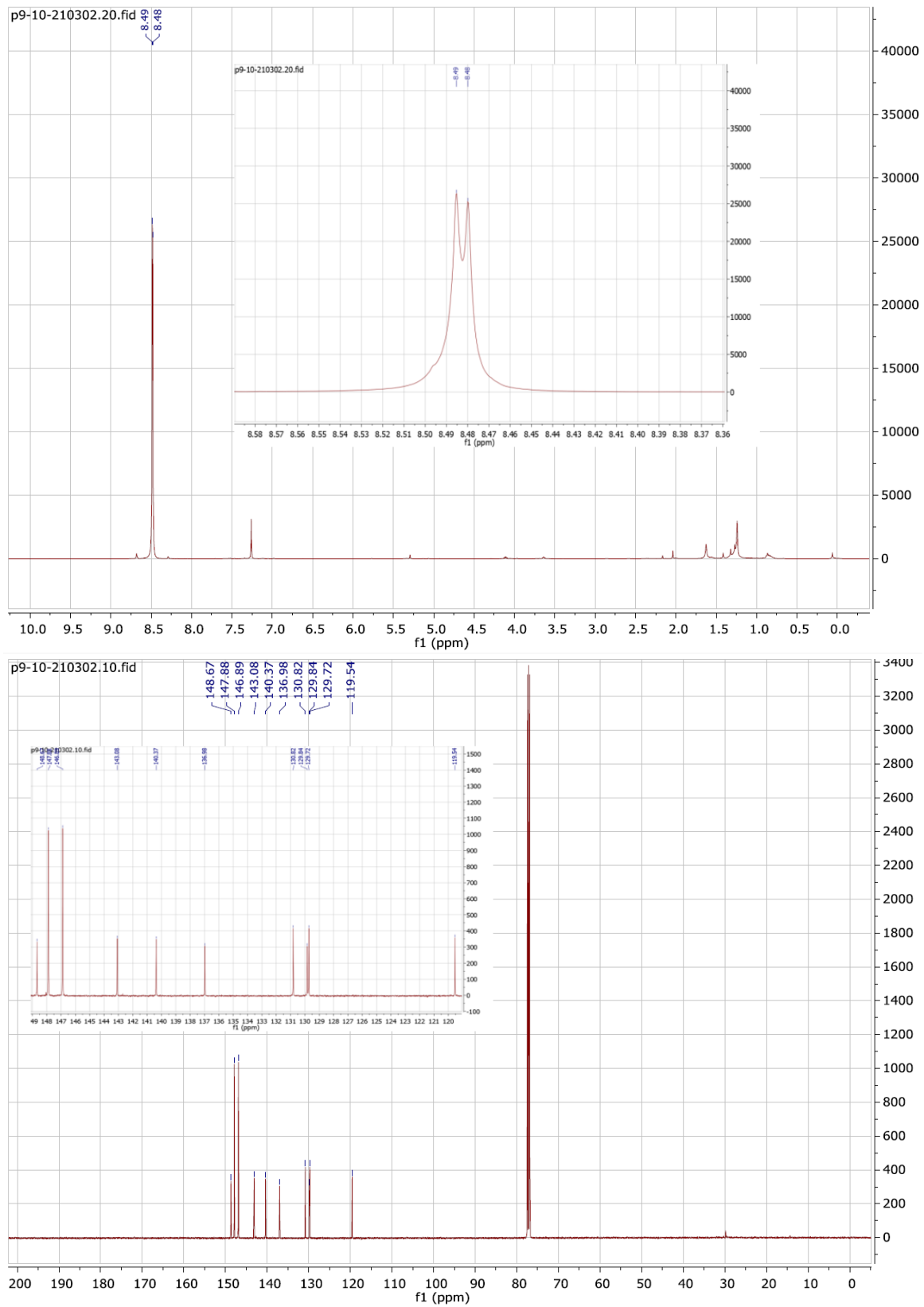


Figure S11. 2,3,3',5,5'-Pentachloro-2'-iodo-4,4'-bipyridine (22).

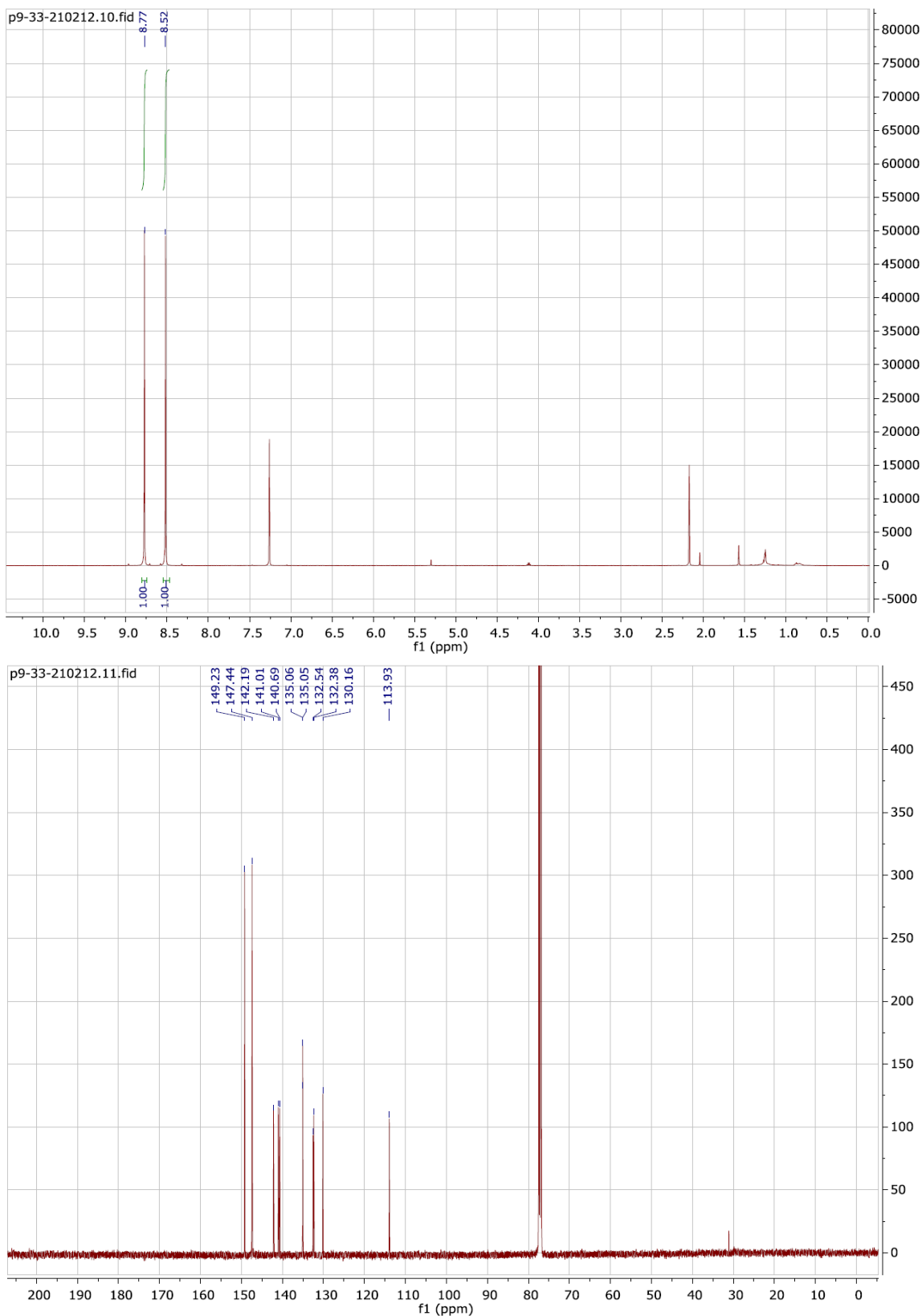


Figure S12. 2'-Bromo-3,3',5,5'-tetrachloro-[4,4'-bipyridine]-2-carbonitrile (**23**).

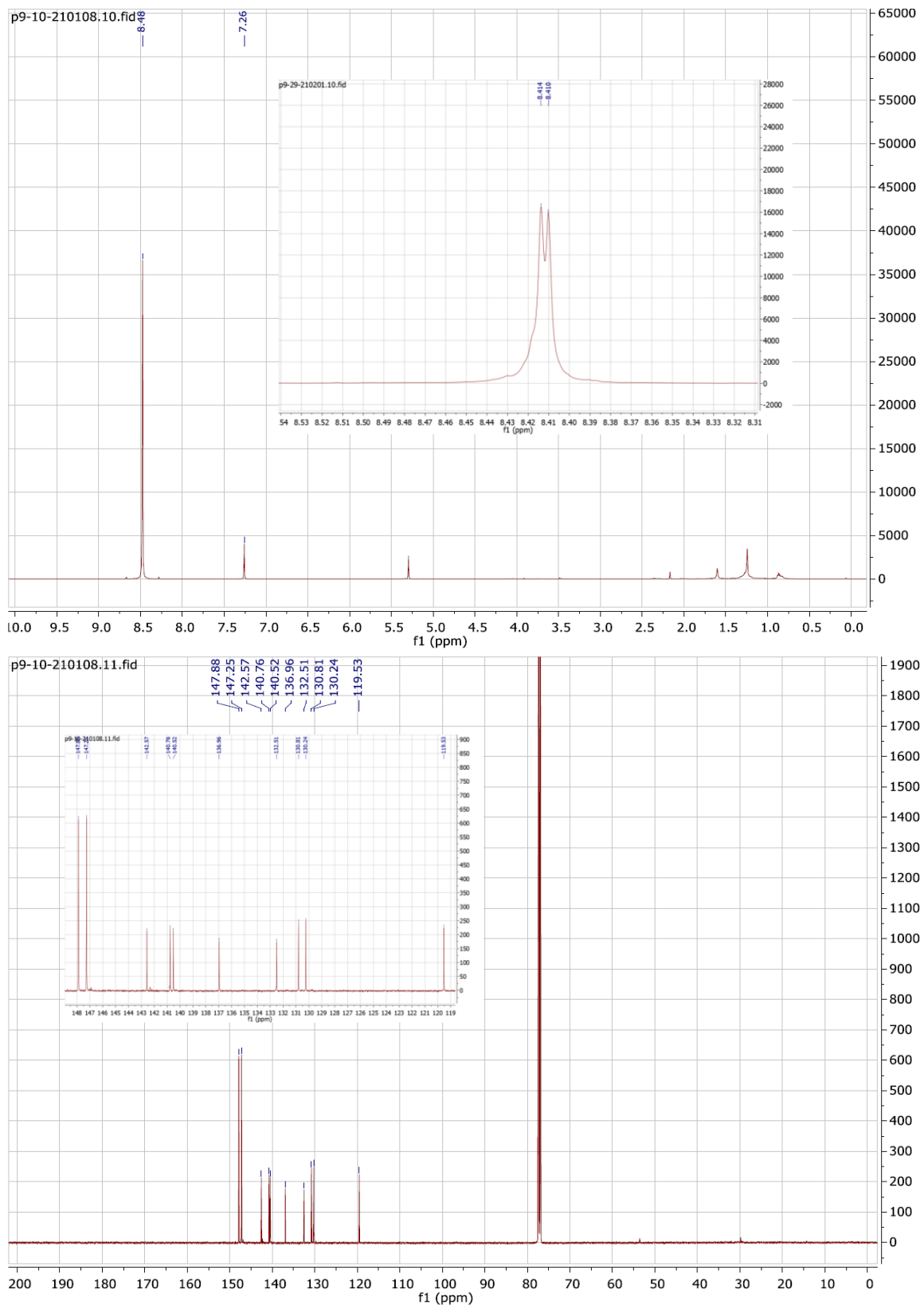


Figure S13. 2-Bromo-3,3',5,5'-tetrachloro-2'-iodo-4,4'-bipyridine (24).

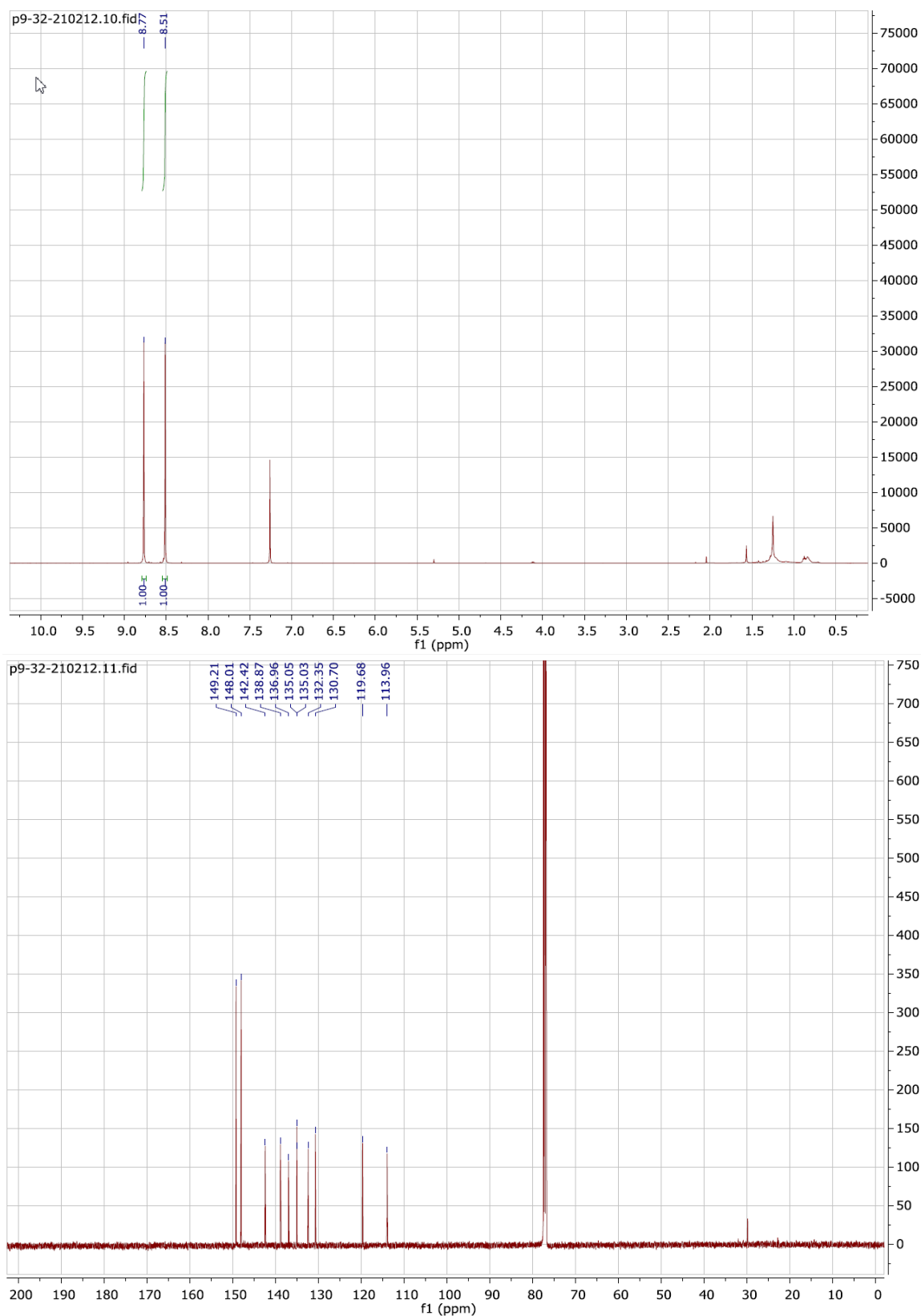


Figure S14. 3,3',5,5'-Tetrachloro-2'-iodo-[4,4'-bipyridine]-2-carbonitrile (**25**).

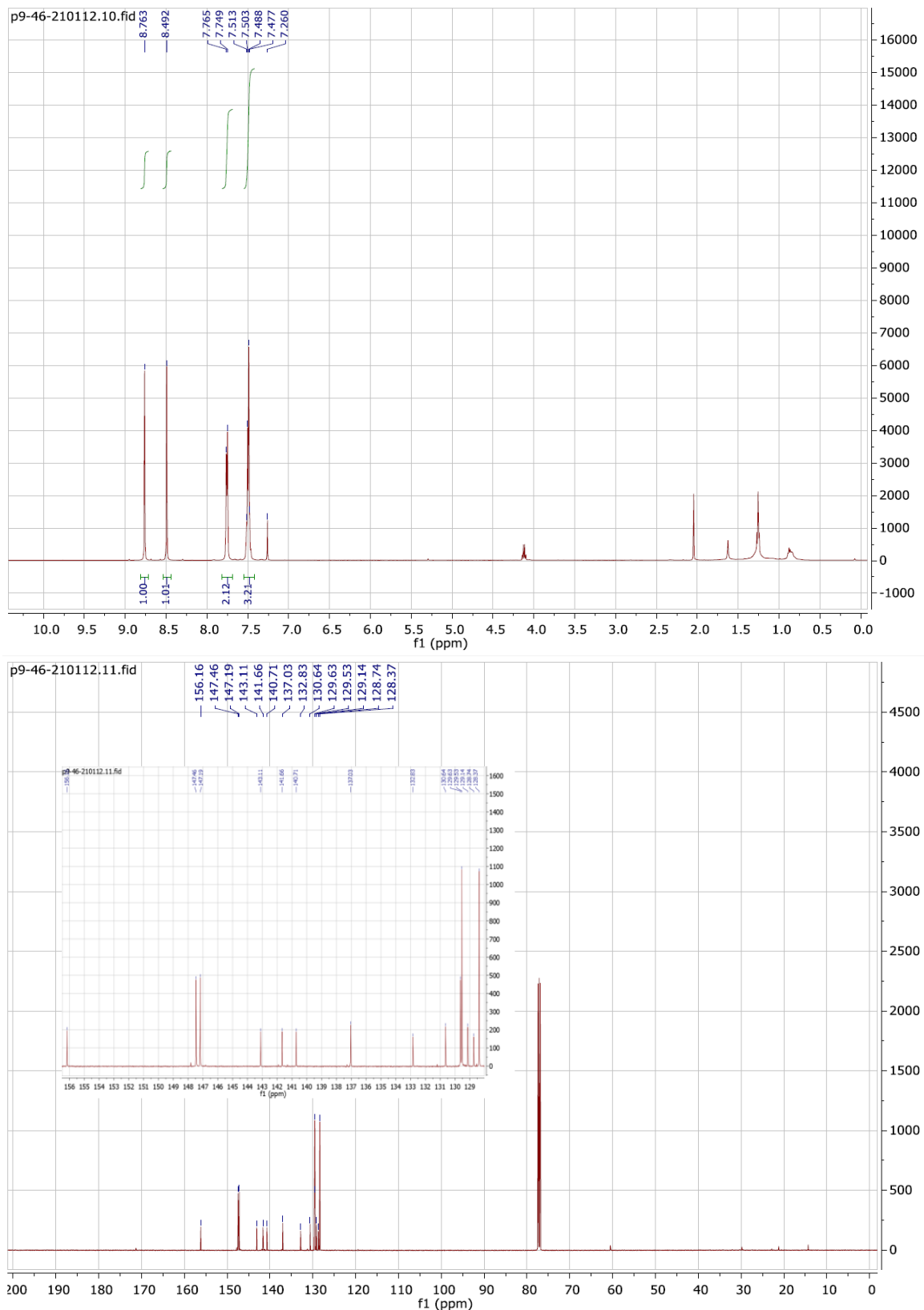


Figure S15. 2-Bromo-3,3',5,5'-tetrachloro-2'-phenyl-4,4'-bipyridine (**26**).

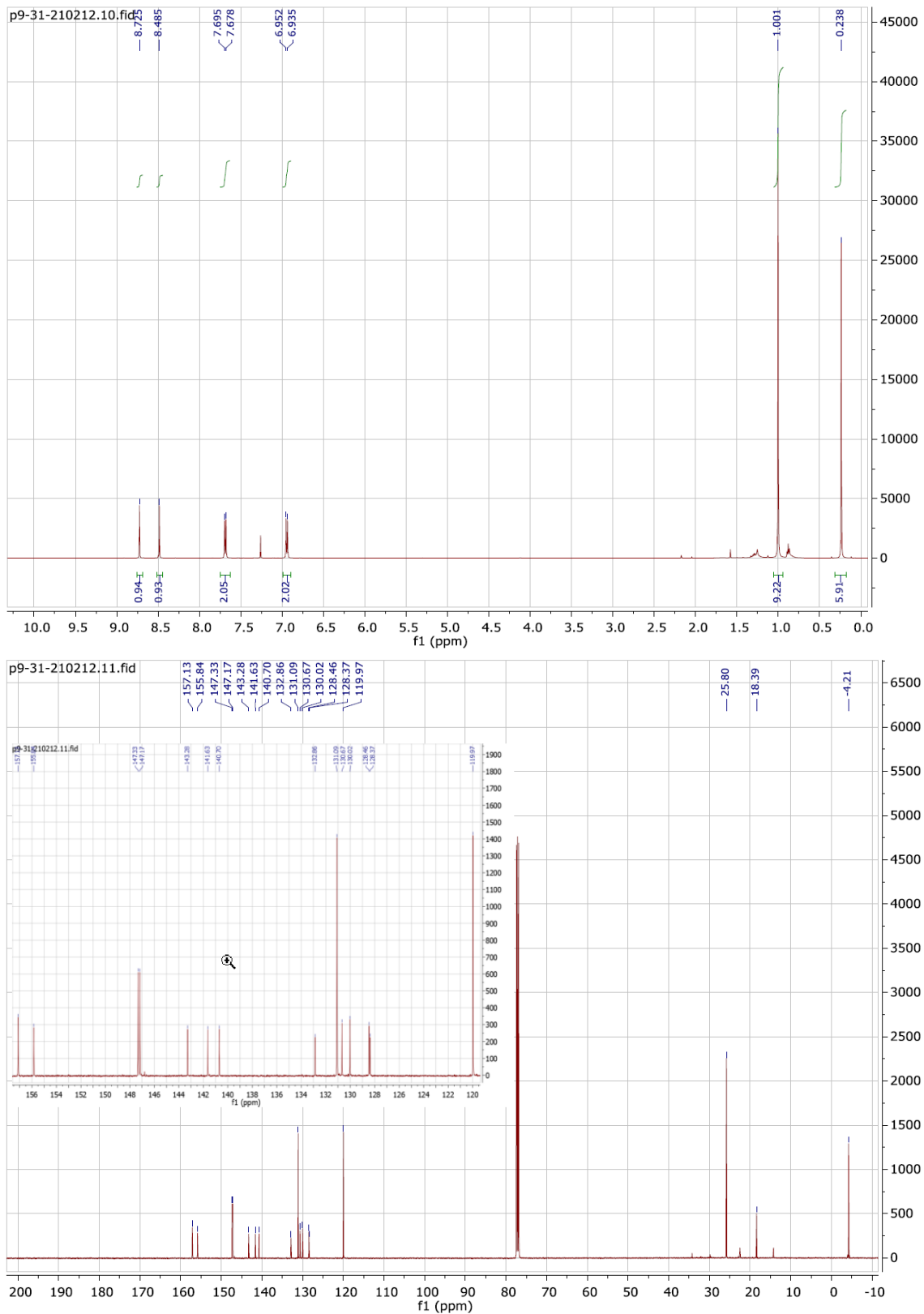


Figure S16. 2-Bromo-2'-(4-((tert-butyldimethylsilyl)oxy)phenyl)-3,3',5,5'-tetrachloro-4,4'-bipyridine (**27**).

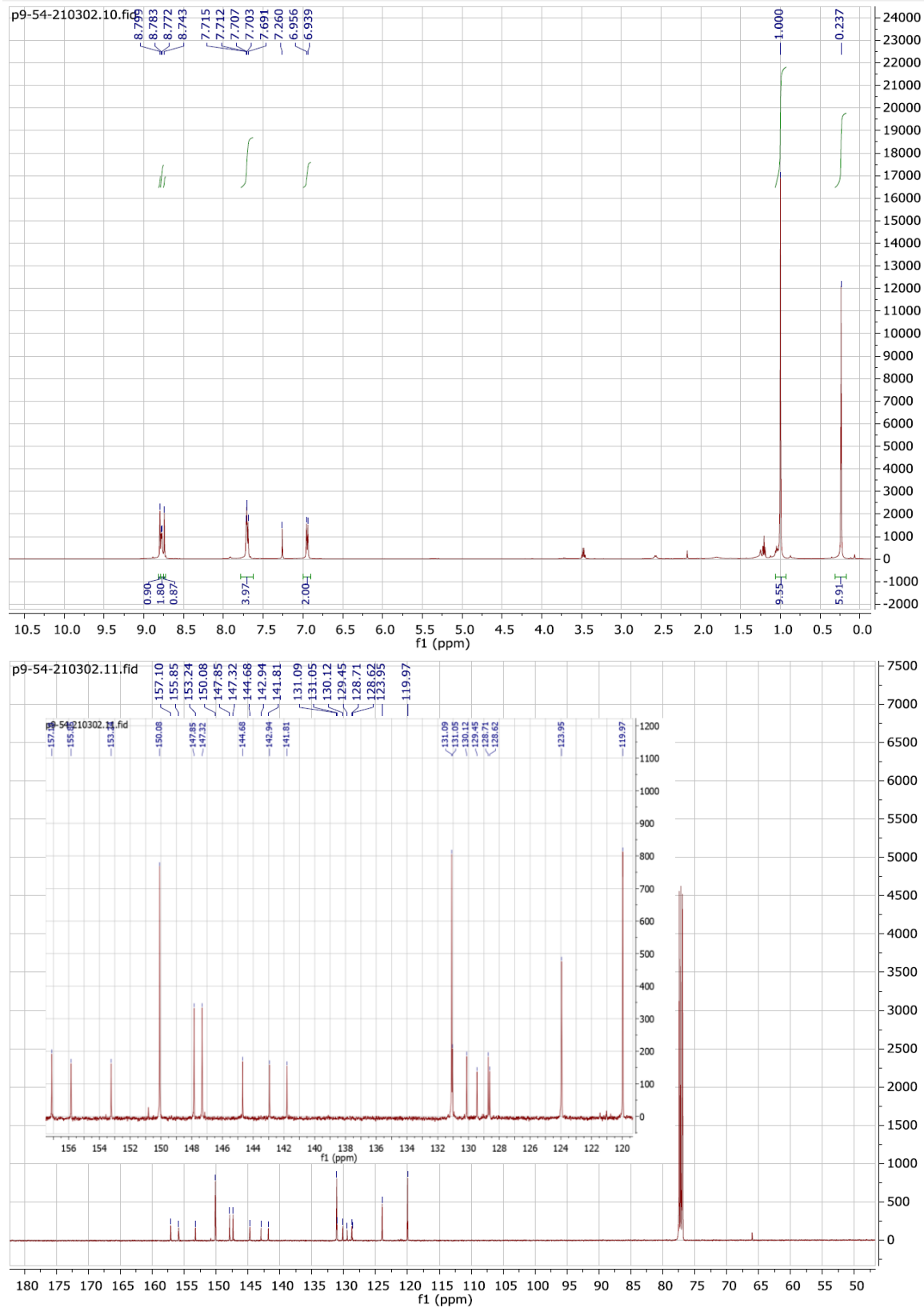


Figure S17. 2''-(4-((Tert-butyldimethylsilyl)oxy)phenyl)-3'',3'',5'',5''-tetrachloro-4,2':4',4''-terpyridine (**31**).

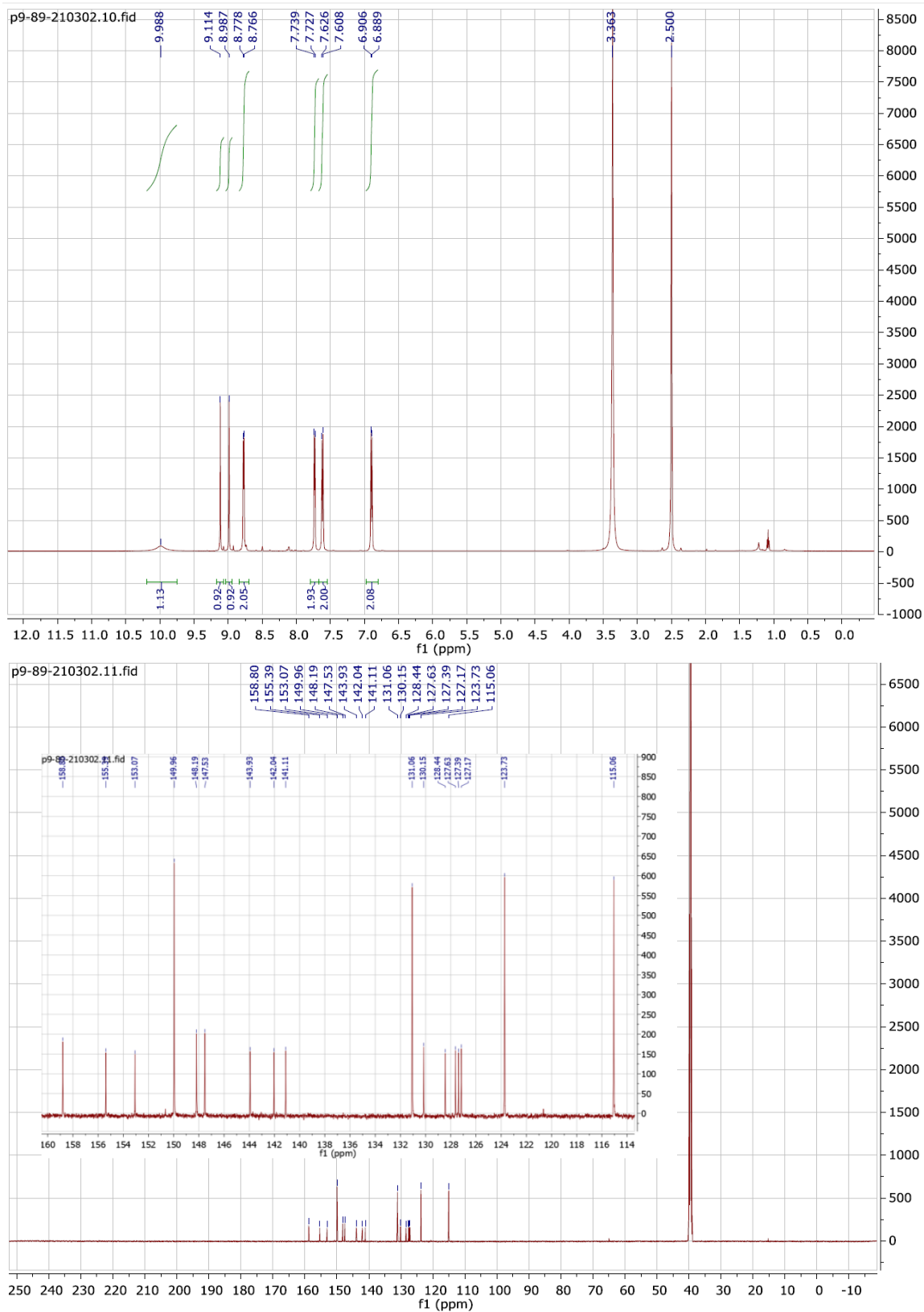


Figure S18. 4-(3',3'',5',5''-Tetrachloro-[4,2':4'4''-terpyridin]-2''-yl)phenol (**32**).

S2. X-Ray Diffraction

Table S1. Intermolecular interaction energies (kJ/mol) in the packing of solid state structure of **24**. R is the distance between molecular centroids (mean atomic position) in Å.

| Entry | Sym. op. | R | E_ele | E_pol | E_dis | E_rep | E_tot |
|-------|--------------------|-------|-------|-------|-------|-------|-------|
| 1 | 2-x, 1-y, 1-z | 7.82 | -22.6 | -1.2 | -37.1 | 28.0 | -32.9 |
| 2 | x, -y+3/2, z-1/2 | 6.82 | -19.3 | -0.4 | -36.9 | 30.2 | -26.6 |
| 3 | 1+x, -y+3/2, z+1/2 | 9.21 | -18.6 | -1.6 | -21.3 | 18.5 | -23.0 |
| 4 | 1-x, 1-y, 1-z | 5.96 | -25.9 | -0.3 | -31.6 | 36.1 | -21.8 |
| 5 | -1+x, y, z | 7.93 | -5.8 | -0.4 | -15.7 | 11.1 | -10.8 |
| 6 | 1-x, y+1/2, -z+1/2 | 8.10 | 0.3 | -0.3 | -9.6 | 4.9 | -4.5 |
| 7 | -1+x, y, -1+z | 12.08 | -11.9 | -0.4 | -6.1 | 16.5 | -1.9 |

Table S2. Intermolecular interaction energies (kJ/mol) in the packing of solid state structure of **18**. Largest differences between **18** and **13** are highlighted in bold. R is the distance between molecular centroids (mean atomic position) in Å.

| Entry | Sym. op. | R | E_ele | E_pol | E_dis | E_rep | E_tot |
|-------|----------------------|-------------|--------------|-------------|--------------|-------------|--------------|
| 1 | 1-x, 1-y, -z | 9.87 | -44.2 | -6.8 | -12.8 | 28.1 | -35.7 |
| 2 | 2-x, 1-y, 1-z | 8.37 | -29.2 | -3.7 | -27.2 | 29.0 | -31.0 |
| 3 | 1-x, 1-y, 1-z | 7.04 | -20.5 | -2.8 | -24.9 | 22.7 | -25.5 |
| 4 | 1+x, -y+3/2, z+1/2 | 10.15 | -21.4 | -2.3 | -8.8 | 7.8 | -24.7 |
| 5 | x, -y+3/2, z-1/2 | 7.52 | -15.7 | -2.0 | -22.4 | 19.5 | -20.6 |
| 6 | 1-x, y+1/2, -z+1/2 | 6.52 | -13.0 | -1.2 | -27.5 | 21.4 | -20.3 |
| 7 | -1+x, y, z | 7.27 | -1.8 | -0.6 | -13.4 | 7.8 | -8.0 |
| 8 | 2-x, y+1/2, -z+1/2 | 8.33 | -1.9 | -0.3 | -6.2 | 6.5 | -1.9 |
| 9 | 2-x, 2-y, 1-z | 11.01 | 2.4 | -0.3 | -1.8 | 0.1 | 0.4 |

Table S3. Intermolecular interaction energies (kJ/mol) in the packing of solid state structure of **13**. Largest differences between **18** and **13** are highlighted in bold. R is the distance between molecular centroids (mean atomic position) in Å.

| Entry | Sym. op. | R | E_ele | E_pol | E_dis | E_rep | E_tot |
|-------|----------------------|-------------|-------------|-------------|--------------|-------------|--------------|
| 1 | 1-x, 1-y, -z | 9.39 | -54.1 | -8.2 | -12.7 | 37.9 | -37.2 |
| 2 | 2-x, 1-y, 1-z | 7.93 | -2.4 | -0.3 | -17.9 | 9.3 | -11.3 |
| 3 | 1-x, 1-y, 1-z | 6.88 | -9.0 | -0.1 | -18.6 | 15.4 | -12.3 |
| 4 | 1+x, -y+3/2, z+1/2 | 9.66 | -26.0 | -3.4 | -10.6 | 16.1 | -23.9 |
| 5 | x, -y+3/2, z-1/2 | 7.38 | -9.4 | -1.3 | -18.5 | 12.8 | -16.4 |
| 6 | 1-x, y+1/2, -z+1/2 | 6.23 | -19.4 | -1.0 | -27.7 | 24.4 | -23.7 |
| 7 | -1+x, y, z | 7.27 | -3.7 | -0.2 | -12.3 | 6.3 | -9.9 |
| 8 | 2-x, y+1/2, -z+1/2 | 8.26 | -4.2 | -0.1 | -5.7 | 8.3 | -1.6 |
| 9 | 2-x, 2-y, 1-z | 10.66 | 1.7 | -0.1 | -2.4 | 0.2 | -0.7 |

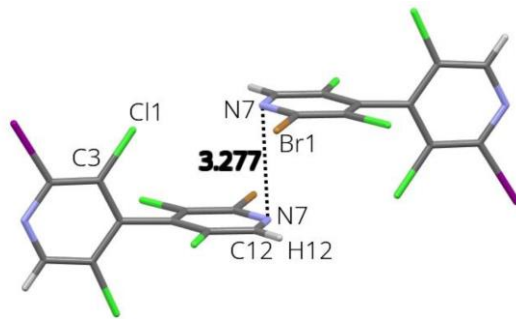


Figure S19. Packing in the solid-state structure of **24**. Interaction between x,y,z , and $2-x, 1-y, 1-z$ molecules. Representative distance is given in Å. Only the major component disorder is shown.

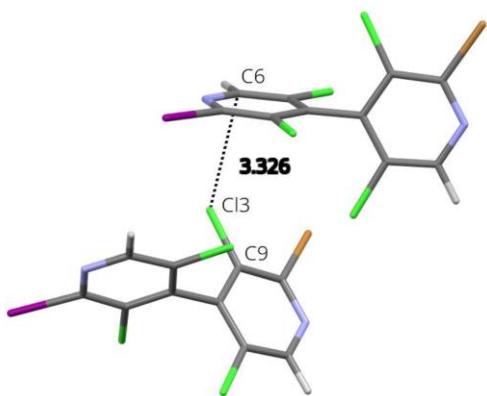


Figure S20. Packing in the solid-state structure of **24**. Interaction between x,y,z , and $x, -y+3/2, z-1/2$ molecules. Representative distance is given in Å. Only the major component disorder is shown.

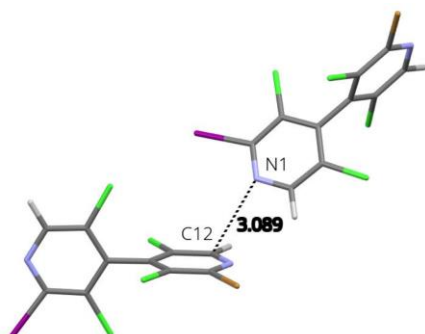


Figure S21. Packing in the solid-state structure of **24**. Interaction between x,y,z , and $1+x, -y+3/2, z+1/2$ molecules. Representative distance is given in Å. Only the major component disorder is shown.

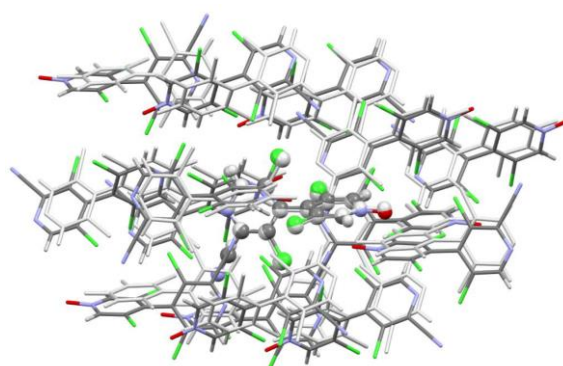


Figure S22. Superimposition of the molecular environment about a central molecule (displayed as ball and sticks) showing the isostructural relationship between **18** (colored as atom type) and **13** (light gray).

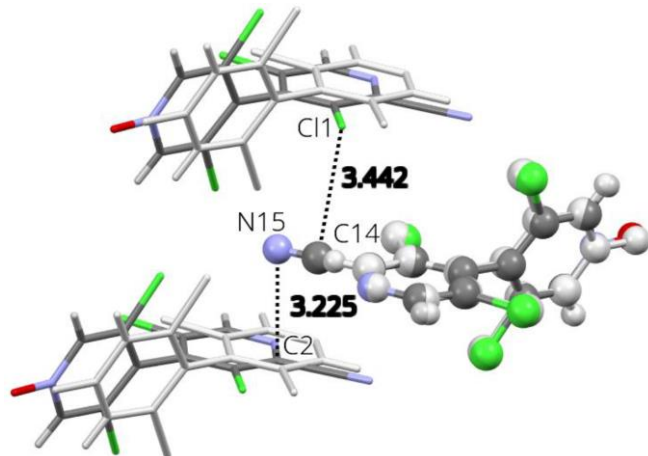


Figure S23. Focus on the region centered on $-CN$ group in **18**, showing the largest differences between **18** (colored as atom type) and **13** (light gray) crystal structures.

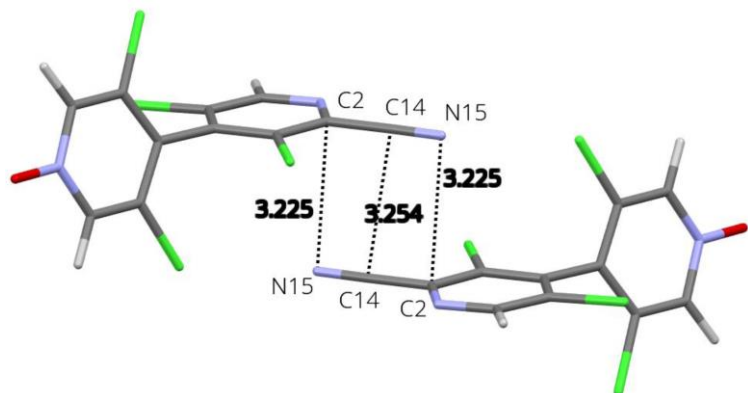


Figure S24. Packing in the solid-state structure of **18**. Interaction between x,y,z , and $2-x, 1-y, 1-z$ molecules. Representative distances are given in Å.

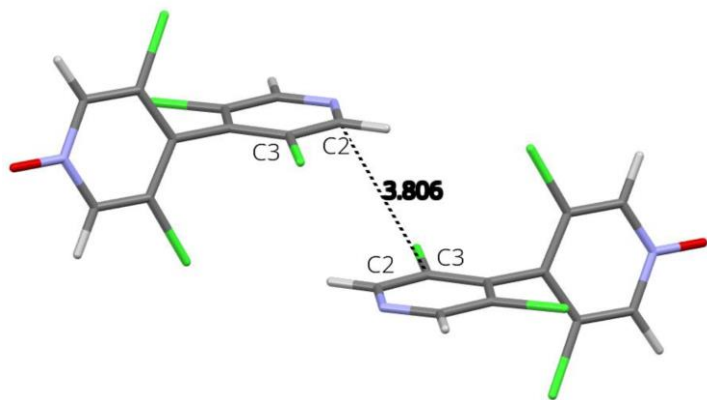


Figure S25. Packing in the solid-state structure of **13**. Interaction between x,y,z , and $2-x, 1-y, 1-z$ molecules. Representative distance is given in Å.

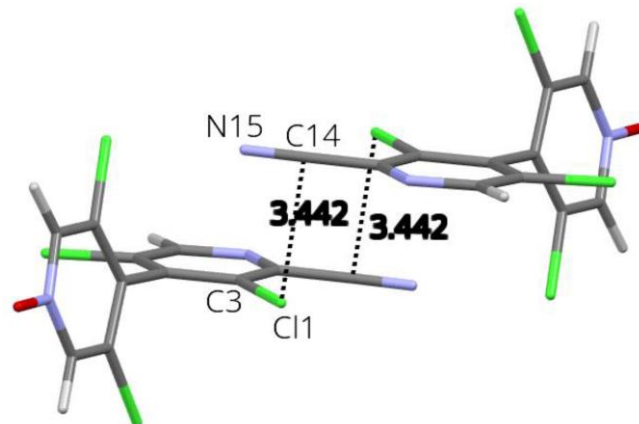


Figure S26. Packing in the solid-state structure of **18**. Interaction between x, y, z , and $1-x, 1-y, 1-z$ molecules. Representative distances are given in Å.

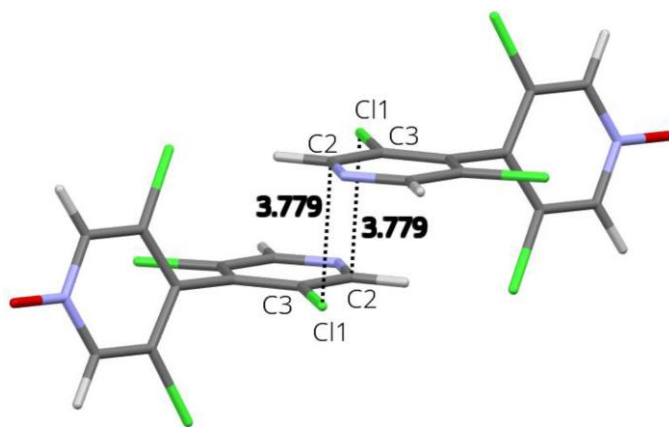


Figure S27. Packing in the solid-state structure of **13**. Interaction between x, y, z , and $1+x, -y+3/2, z+1/2$ molecules. Representative distances are given in Å.

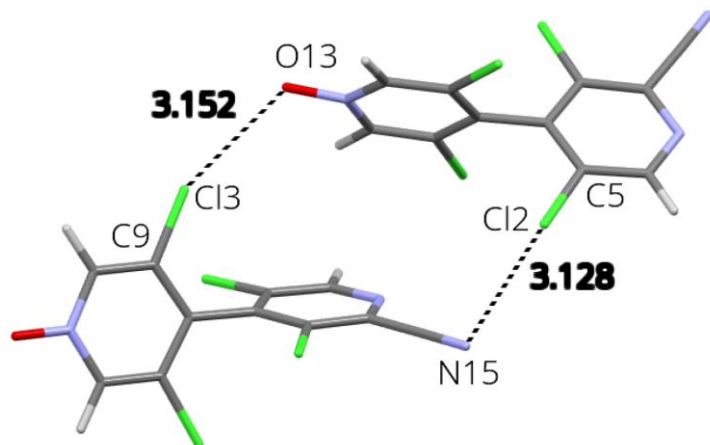


Figure S28. Packing in the solid-state structure of **18**. Interaction between x, y, z , and $x, -y+3/2, z-1/2$ molecules. Representative distances are given in Å.

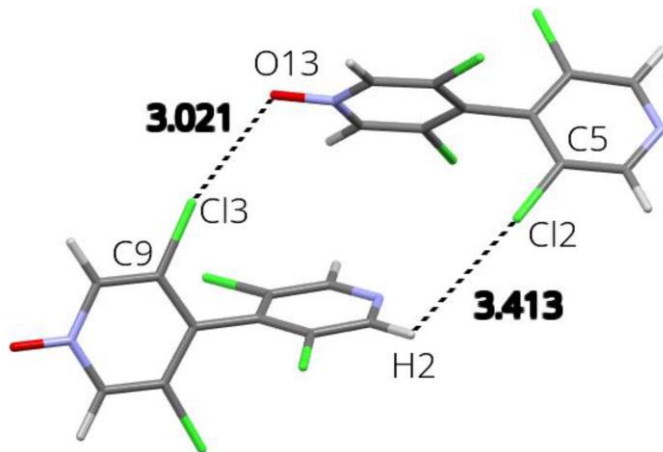


Figure S29. Packing in the solid-state structure of **13**. Interaction between x,y,z , and $x, -y+3/2, z-1/2$ molecules. Representative distances are given in Å.

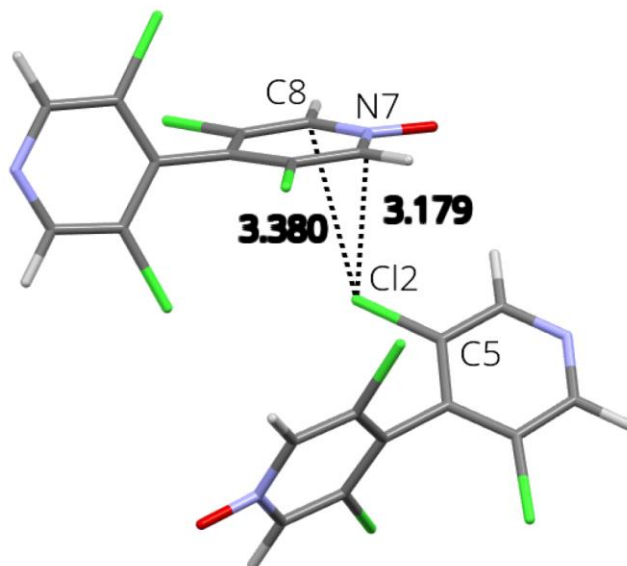


Figure S30. Packing in the solid-state structure of **13**. Interaction between x,y,z , and $1-x, y+1/2, -z+1/2$ molecules. Representative distances are given in Å.

S3 Theoretical Calculations

Table S4. Electrostatic potential maxima ($V_{S,\max}$; kcal/mol) on the molecular surface $\rho = 0.002$ a.u. of **24**.

| Atomic Site | $V_{S,\max}$ |
|--|-------------------------|
| I1 | 32.54 |
| H12 | 32.08 |
| H6 | 31.87 |
| Cl4/Cl2/Cl3/Cl1 | 23.38/23.35/23.00/22.92 |
| Br1 | 22.69 |
| π -holes (BrI/BrH/IBr/IH) ^a | 21.89/21.84/21.39/21.37 |

^a π -holes XY are identified as belonging to the pyridine ring bearing X halogen, on the side of Y atom of the second pyridine ring.

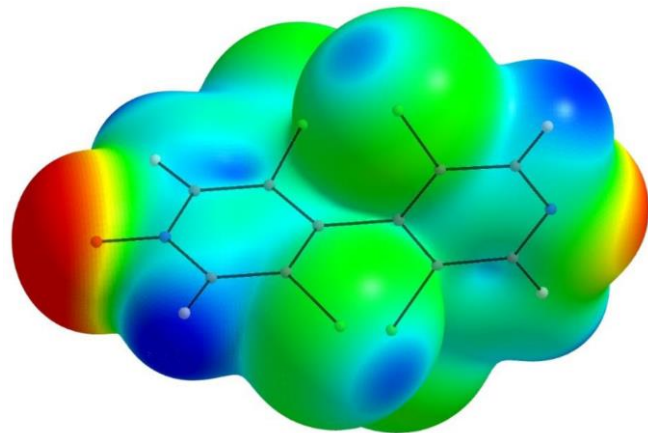


Figure S31. Electrostatic potential mapped on the $\rho = 0.002$ a.u. electron density isosurface of **13**.
Coloring from red = -0.05 a.u. to blue = $+0.05$ a.u.

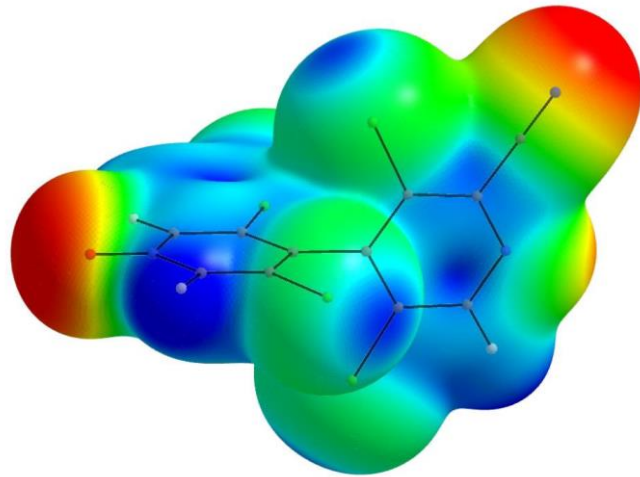


Figure S32. Electrostatic potential mapped on the $\rho = 0.002$ a.u. electron density isosurface of **18**.
Coloring from red = -0.05 a.u. to blue = $+0.05$ a.u.

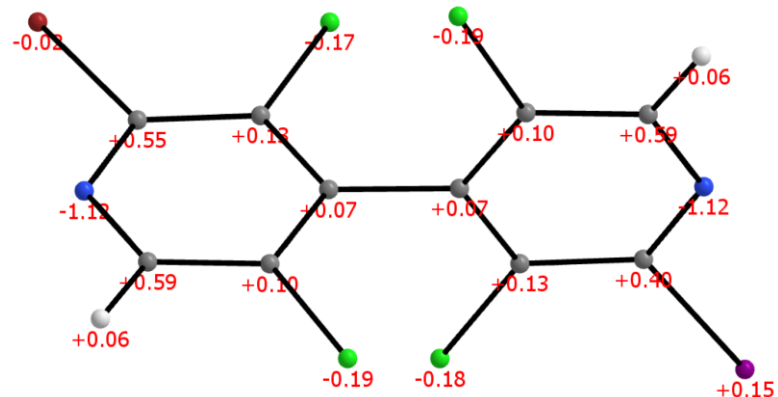


Figure S33. Integrated Bader atomic charges for isolated **24** molecule.

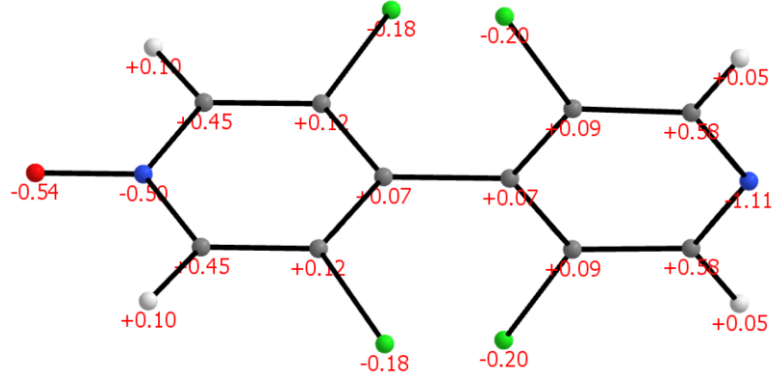


Figure S34. Integrated Bader atomic charges for isolated **13** molecule.

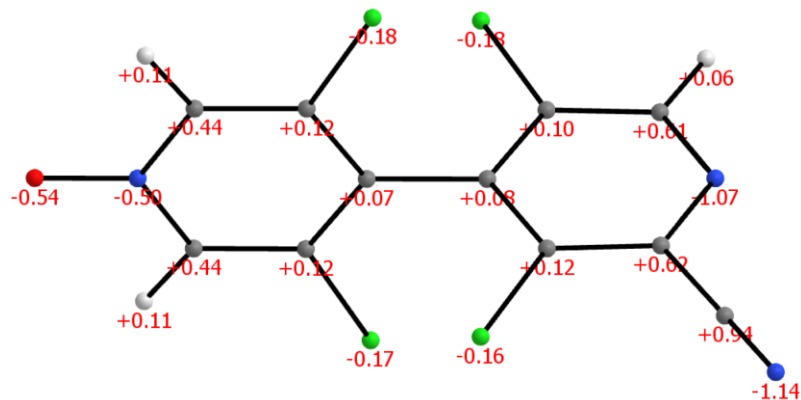


Figure S35. Integrated Bader atomic charges for isolated **18** molecule.

Study of the Type-II Hal···Hal Interactions in **24**

The four molecules ($x,y,z; -1+x,y,-1+z; -x,1-y,-z; 1-x,1-y,1-z$) forming a cyclic four membered ring of type-II Hal···hal interactions (Figure S18) were extracted from the crystal structure of **24**. All possible configurations corresponding to positions of I and Br were constructed with Hal1-4=I or Br and HalX' being Br if HalX=I and conversely. For each generated terramer the position of iodine, bromine and hydrogen atoms were optimized (B3LYP-D3, Def2TZVPP) while keeping the carbon, nitrogen and chlorine atoms frozen; the resulting final relative energies are listed in Table S5. Boltzmann populations ($T = 293$ K) were then deduced for each configuration, and population for each $\text{Hal}X = 1-4$ site obtained by proper summations. The fractional iodine occupations obtained are: Hal1 = 0.60; Hal2 = 0.25; Hal3 = 0.60; Hal4 = 0.25 (fractional bromine occupations are complementary to 1.00).

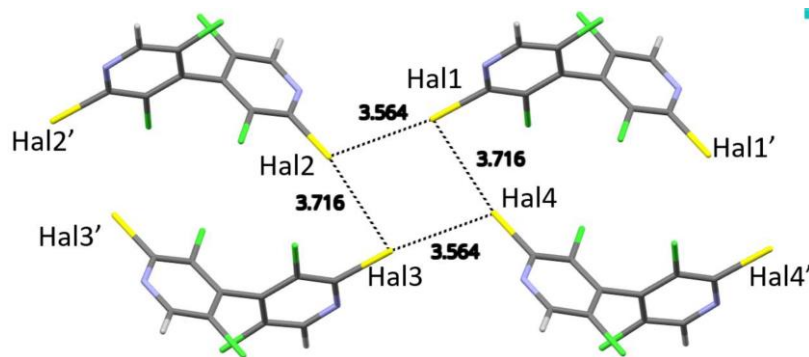


Figure S36. Tertamer extracted from the experimental structure of **24** and used for the modeling of I/Br substitution disorder. $\text{Hal}X/\text{Hal}X'$ are I/Br or Br/I.

Table S5. Type-II hal··hal bonds four membered ring tetramer relative energies. Hal1-2-3-4 numbering corresponds to Figure S18.

| Hal1-2-3-4 | ΔE (kJ/mol) |
|------------------------------------|---------------------|
| I ⁻ BrI ⁻ Br | 0.00 |
| BrBrI ⁻ Br | 2.10 |
| I ⁻ BrBrBr | 2.11 |
| BrBrBrBr | 3.98 |
| BrBrII | 4.21 |
| IIBrBr | 4.23 |
| BrIBrBr | 4.54 |
| BrBrBrI | 4.55 |
| IIIBr | 4.56 |
| IBrII | 4.57 |
| BrIBrI | 4.80 |
| BrIIBr | 5.19 |
| IBrBrI | 5.21 |
| BrIII | 7.08 |
| IIBrI | 7.08 |
| III | 8.92 |

From the single crystal X-ray structure determination a fractional occupancy of 0.7441(13) is obtained for iodine on sites Hal1 and Hal3 (related by the inversion center), and of 0.2559(13) on sites Hal2 and Hal4 (complementary values for bromine atom). The fact that for the tetramer calculations the populations for iodine (or bromine) on sites Hal1 (resp. Hal3) and Hal2 (resp. Hal4) are not complementary comes from the fact that no translational symmetry is imposed during these calculations (e.g. x,y,z and $-1+x,y,-1+z$), contrarily to what is done during the experimental X-ray structure refinement. The global iodine population average over all sites ($(0.60+(1-0.25))/2 = 0.675$) is close to the experimentally obtained population (0.7441(13)).

References

1. M. J. Turner, J. J. McKinnon, S. K. Wolff, D. J. Grimwood, P. R. Spackman, D. Jayatilaka and M. A. Spackman, CrystalExplorer17 (2017). University of Western Australia. <https://hirshfeldsurface.net>.
2. AIMAll (Version 19.10.12), Todd A. Keith, TK Gristmill Software, Overland Park KS, USA, 2019 (aim.tkgristmill.com)
3. Gaussian 09, Revision D.01, M. J. Frisch, G. W. Trucks, H. B. Schlegel, G. E. Scuseria, M. A. Robb, J. R. Cheeseman, G. Scalmani, V. Barone, B. Mennucci, G. A. Petersson, H. Nakatsuji, M. Caricato, X. Li, H. P. Hratchian, A. F. Izmaylov, J. Bloino, G. Zheng, J. L. Sonnenberg, M. Hada, M. Ehara, K. Toyota, R. Fukuda, J. Hasegawa, M. Ishida, T. Nakajima, Y. Honda, O. Kitao, H. Nakai, T. Vreven, J. A. Montgomery, Jr., J. E. Peralta, F. Ogliaro, M. Bearpark, J. J. Heyd, E. Brothers, K. N. Kudin, V. N. Staroverov, T. Keith, R. Kobayashi, J. Normand, K. Raghavachari, A. Rendell, J. C. Burant, S. S. Iyengar, J. Tomasi, M. Cossi, N. Rega, J. M. Millam, M. Klene, J. E. Knox, J. B. Cross, V. Bakken, C. Adamo, J. Jaramillo, R. Gomperts, R. E. Stratmann, O. Yazyev, A. J. Austin, R. Cammi, C. Pomelli, J. W. Ochterski, R. L. Martin, K. Morokuma, V. G. Zakrzewski, G. A. Voth, P. Salvador, J. J. Dannenberg, S. Dapprich, A. D. Daniels, O. Farkas, J. B. Foresman, J. V. Ortiz, J. Cioslowski, and D. J. Fox, Gaussian, Inc., Wallingford CT, 2013.
4. Tian Lu & Feiwu Chen. *Comput. Chem.*, **33**, 580-592 (2012)